Journal of Materials Chemistry A

PAPER

View Article Online
View Journal | View Issue

Cite this: J. Mater. Chem. A, 2015, 3, 555

In situ formed carbon bonded and encapsulated selenium composites for Li–Se and Na–Se batteries†

Chao Luo,[a] Jingjing Wang,[b] Liumin Suo,[a] Jianfeng Mao,[a] Xiulin Fan[a] and Chunsheng Wang*[a]

Received 5th September 2014
Accepted 28th October 2014

DOI: 10.1039/c4ta04611k

www.rsc.org/MaterialsA

As high capacity cathodes for Li-ion and Na-ion batteries, carbon bonded and encapsulated selenium composites (C/Se) with a high loading content of 54% Se were synthesized by the *in situ* carbonization of a mixture of perylene-3,4,9,10-tetracarboxylic dianhydride (PTCDA) and selenium (Se) in a sealed vacuum glass tube. Because Se is physically encapsulated and chemically bonded by carbon, the shuttle reaction of polyselenide is effectively mitigated. The *in situ* formed C/Se composites exhibit superior cycling stability for both Li-ion and Na-ion batteries in carbonate-based electrolytes. The reversible capacity of the *in situ* formed C/Se composites is maintained at 430 mA h g^{-1} after 250 cycles in Li-ion batteries and 280 mA h g^{-1} after 50 cycles in Na-ion batteries at a current density of 100 mA g^{-1}.

Introduction

Emerging electric vehicles and smart grids require high power and high capacity energy storage devices.[1] The primary technological bottleneck of state-of-the-art Li-ion and Na-ion batteries appears due to the low energy density of ceramic cathodes, which cannot satisfy the critical energy requirement of electric vehicles and smart grids.[2–4] Even though lithium rich metal oxides, which attract considerable research interest due to its higher capacity than the commercial lithium metal oxide, can deliver only a reversible capacity of 250 mA h g^{-1};[5,6] it still cannot match with its anode counterparts such as graphite, Sn and Si.[7–10]

To date, sulfur is the most promising cathode material due to its abundance, high theoretical capacity (1675 mA h g^{-1}) and low cost.[11–13] However, lithium sulfur batteries suffer from two major challenges:[14–17] (1) the insulating nature of sulfur results in the low utilization of sulfur cathodes and the sluggish kinetics of lithium sulfur batteries; (2) severe shuttle reaction, triggered by the formation of high solubility polysulfide intermediates during the lithiation/delithiation process, results in rapid capacity fading. Although tremendous advances in stabilizing sulfur cathodes have been achieved *via* carbon coating and nanomaterial fabrication,[18–22] the two challenges still cannot be resolved, and sulfur cannot be commercialized as cathodes in Li-ion and Na-ion batteries.

The recent investigation on selenium provides new opportunities to develop advanced cathode materials for lithium and sodium storage. Abouimrane *et al.* reported that selenium, the congener of sulfur, is a promising cathode material for both lithium ion and sodium ion batteries due to the comparable volumetric capacity (3253 Ah L^{-1}) to sulfur (3467 Ah L^{-1}).[23–25] Though Se cathodes suffer from similar dissolution issues as sulfur, its higher electrical conductivity than sulfur is advantageous because it may increase the utilization and power density of Se cathodes. In selenium cathodes, porous carbon as a conductive framework was used to encapsulate Se, thus circumventing the shuttle reaction.[26,27] Carbon coated Se, nanofibrous Se, free standing graphene/Se film and TiO_2–Se composite were also reported to demonstrate improved electrochemical performance.[28–35] In our previous work, we impregnated Se into mesoporous carbon, which delivered a reversible capacity of 480 mA h g^{-1} for 1000 cycles without any capacity loss in Li-ion batteries, and 340 mA h g^{-1} for 380 cycles in Na-ion batteries.[36] The exceptional battery performance is ascribed to the synergic physical encapsulation by porous carbon and solid-electrolyte-interphase (SEI) formed from the reduction of a carbonate-based electrolyte. Though such excellent electrochemical performance is achieved by filling Se into mesoporous carbon, the low loading content (30%) of Se in the composite impedes its widespread application in rechargeable batteries.

In this study, C/Se composites containing 54% of Se were *in situ* synthesized by annealing a mixture of PTCDA and Se in a sealed vacuum glass tube, as shown in Fig. 1. One PTCDA molecule contains six oxygen atoms, which are active sites to

[a]Department of Chemical and Biomolecular Engineering, University of Maryland, College Park, MD 20742, USA. E-mail: cswang@umd.edu

[b]Department of Chemistry and Biochemistry, University of Maryland, College Park, MD 20742, USA

† Electronic supplementary information (ESI) available. See DOI: 10.1039/c4ta04611k

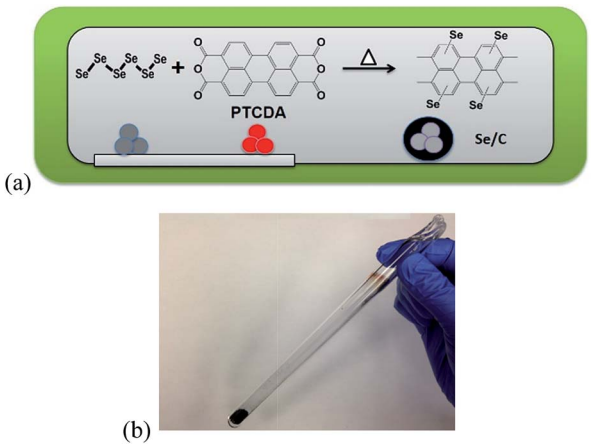

Fig. 1 (a) Schematic illustration for the *in situ* synthesis of C/Se composites; and (b) image of sealed vacuum glass tube after annealing.

react with selenium at high temperatures. The resulting C/Se composites were collected as a black powder (Fig. 1b) in the vacuum glass tube after annealing at 600 °C. The high temperature treatment enables the chemical bonding and physical encapsulation of Se by carbon. The *in situ* formed C/Se composites exhibit a very stable cycling performance in commercial carbonate based electrolytes. The C/Se composites with a high loading content of Se maintains a reversible capacity of 430 mA h g^{-1} after 250 cycles in Li-ion batteries and 280 mA h g^{-1} after 50 cycles in Na-ion batteries.

Experimental

Synthesis of C/Se composites

All the chemicals were purchased from Sigma Aldrich and used as received. Selenium and perylene-3,4,9,10-tetracarboxylic-dianhydride were mixed in a ratio of 1.5 : 1 by weight and sealed in a glass tube under vacuum. The sealed glass tube was annealed in an oven at 600 °C for 3 h, and it was cooled to room temperature over 24 h. The C/Se composites were collected as a black powder.

Material characterization

Scanning electron microscopy (SEM) images were obtained by a Hitachi SU-70 analytical ultra-high resolution SEM (Japan); transmission electron microscopy (TEM) images were obtained by a JEOL (Japan) 2100F field emission TEM; thermogravimetric analysis (TGA) was carried out using a thermogravimetric analyzer (TA Instruments, USA) with a heating rate of 10 °C min^{-1} in argon; X-ray diffraction (XRD) pattern was recorded by a Bruker Smart1000 (Bruker AXS Inc., USA) using CuKα radiation; Raman measurements were performed on a Horiba Jobin Yvon Labram Aramis using a 532 nm diode-pumped solid-state laser, attenuated to give ~900 μW power at the sample surface. X-ray photoelectron spectroscopy (XPS) analysis was performed on a high sensitivity Kratos AXIS 165 X-ray photoelectron spectrometer using monochronic AlKα radiation.

Electrochemical measurements

The *in situ* formed C/Se composites were mixed with carbon black and sodium alginate binder to form a slurry with a weight ratio of 80 : 10 : 10. The electrode was prepared by casting the slurry onto aluminum foil using a doctor blade, and the electrode was dried overnight in a vacuum oven at 60 °C. The slurry coated on aluminum foil was punched into circular electrodes with an area mass loading of 1.2 mg cm^{-2}. Coin cells for the lithium selenium batteries were assembled with lithium foil as the counter electrode, 1 M $LiPF_6$ in a mixture of ethylene carbonate/diethyl carbonate (EC–DEC, 1 : 1 by volume) and Celgard®3501 (Celgard, LLC Corp., USA) as the separator. Coin cells for the sodium selenium batteries were assembled with sodium metal as the counter electrode, 1 M $NaClO_4$ in a mixture of ethylene carbonate/dimethyl carbonate (EC–DMC, 1 : 1 by volume) and Celgard®3501 (Celgard, LLC Corp., USA) as the separator. Electrochemical performance was tested using an Arbin battery test station (BT2000, Arbin Instruments, USA). Capacity was calculated on the basis of the mass of selenium in the C/Se composites. Cyclic voltammograms were recorded using a Gamry Reference 3000 Potentiostat/Galvanostat/ZRA with a scan rate of 0.1 mV s^{-1}.

Results and discussion

Fig. 2 shows the morphology of the C/Se composites, which consist of irregular shaped particles with a size of about 1 μm. The Se is uniformly distributed in the C/Se composite (Fig. 2b), as demonstrated by the energy dispersive X-ray spectroscopy (EDS) (Fig. 2c and d). The content of Se in the composite was determined by thermogravimetric analysis (TGA), as shown in Fig. S1.† The *in situ* formed C/Se composites contain 54% of Se, which is considerably higher than that (30%) of the Se impregnated mesoporous carbon composite in our previous work.[34]

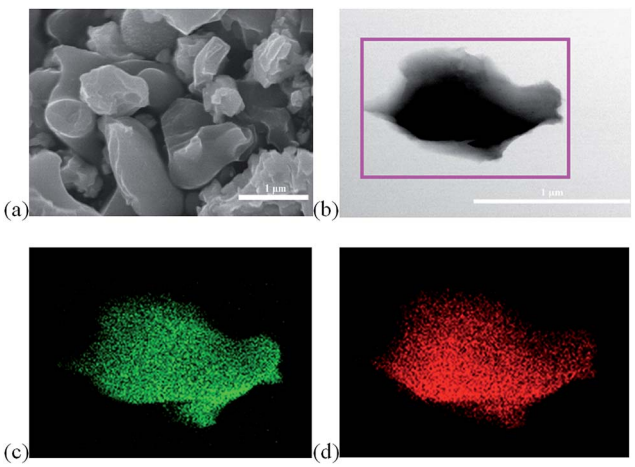

Fig. 2 (a) SEM image of the *in situ* formed C/Se composite; (b) TEM image of the *in situ* formed C/Se composite and EDS elemental mapping images of the composites, marked by the purple square, for carbon (c) and selenium (d).

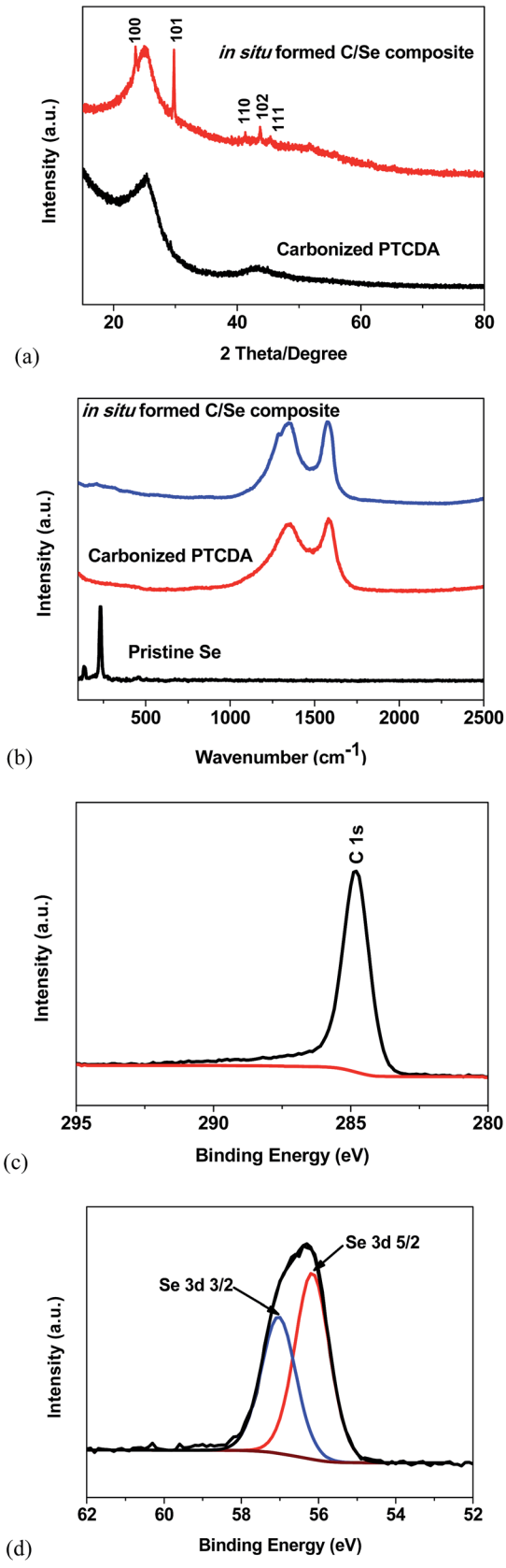

Fig. 3 XRD patterns (a) and Raman spectra (b) for pristine Se, and the *in situ* formed C/Se composite; XPS spectra of the *in situ* formed C/Se composite: (c) C 1s, and (d) Se 3d. Note: the XPS peaks are calibrated using the C 1s peak at 284.8 eV.

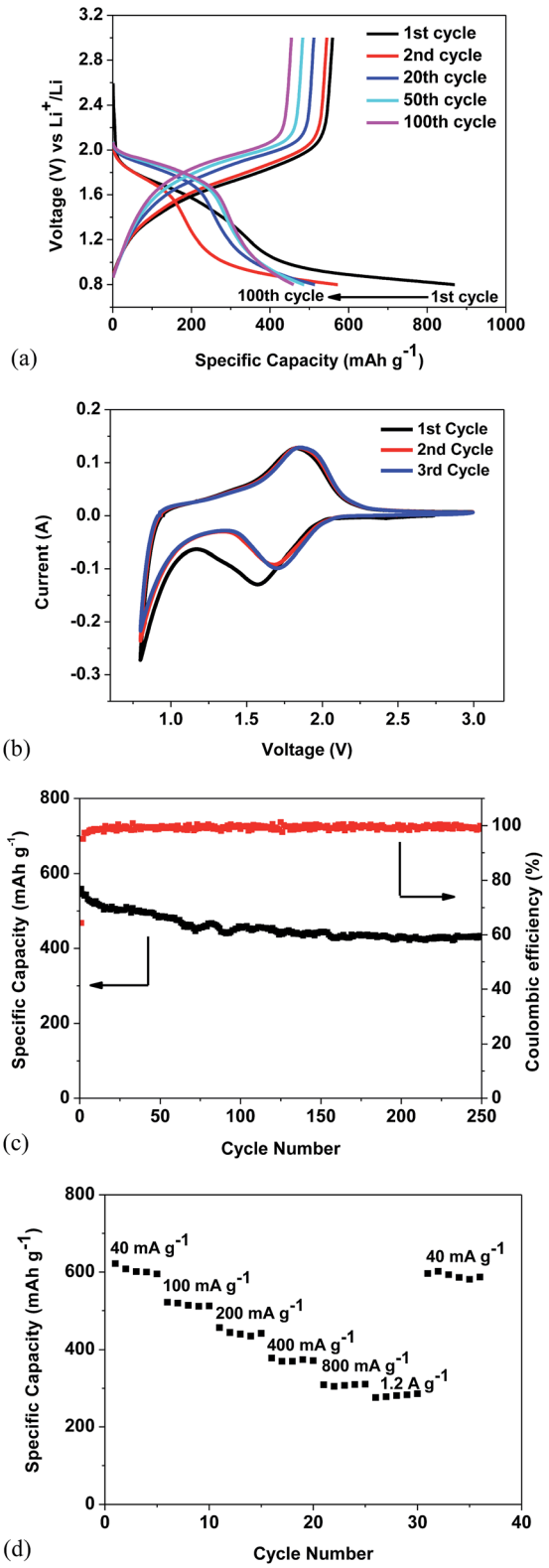

Fig. 4 Electrochemical performance of the *in situ* formed C/Se composite. (a) The galvanostatic charge–discharge curves between 0.8 V and 3.0 V *versus* Li/Li^+; (b) cyclic voltammograms at 0.1 mV s^{-1} in the potential window from 0.8 V to 3.0 V *versus* Li/Li^+; (c) delithiation capacity and coulombic efficiency *versus* cycle number at the current density of 100 mA g^{-1}; and (d) rate performance at various C-rates.

The structure of the C/Se composite was characterized using X-ray diffraction (XRD), as shown in Fig. 3a. It shows a broad peak at 26 degrees with few small peaks. The broad peak at 26 degrees is attributed to graphitic carbon derived from the carbonized PTCDA, whereas the small peaks are indexed to crystalline Se. Because the intensity of the XRD peaks for crystal Se is very weak, it can be inferred that only a small portion of Se exists in the form of crystalline structure.

The nature of the interaction between C and Se was characterized using Raman spectroscopy and X-ray photoelectron spectroscopy (XPS). Se and carbonized PTCDA were used as control samples to identify the Raman spectra of the C/Se composites. Fig. 3b shows the Raman peaks of pristine Se, carbonized PTCDA and the *in situ* formed C/Se composites. Two broad carbon peaks at 1345 cm^{-1} and 1595 cm^{-1}, appearing in both the carbonized PTCDA and C/Se composites, represent the disordered graphite (D band) and crystalline graphite (G band), respectively. The similar peak intensity between the D band and G band in the C/Se composite is indicative of the good electrical conductivity of the carbon matrix derived from the carbonized PTCDA. No Raman peak for pristine Se is observed in the C/Se composites, demonstrating that the small amount of crystal Se is encapsulated by a carbon matrix because Raman spectroscopy only collects signals from the surface of a material. The interaction between C and Se was characterized by XPS, as shown in Fig. 3c and d. The asymmetry of the C 1s peak of the C/Se composite in Fig. 3c indicates the co-existence of sp^2 and sp^3 carbons owing to the graphitic structure of the carbon matrix. The binding energies of elemental Se 3d 5/2 is in the range from 55.1 eV to 55.5 eV. However, the binding energies of Se 3d 3/2 and Se 3d 5/2 in the C/Se composite are located at 57.0 eV and 56.2 eV, respectively, which are higher than that of elemental Se. The high binding energies of Se is attributed to the strong chemical bond between Se and carbon.[37] The unique synthetic technique of using a sealed vacuum glass tube enables the formation of the C–Se bond at high temperatures. The absence of elemental Se in the XPS spectrum further confirms that a small amount of crystal Se is encapsulated by a carbon matrix because XPS collects signals only from the surface of a material. Therefore, the *in situ* formed carbon bonded and encapsulated selenium–carbon composites are obtained by using the unique synthetic technique of a sealed vacuum glass tube.

The electrochemical performances of the C/Se composites in Li-ion battery and Na-ion batteries were measured in coin cells with carbonate-based electrolytes. Fig. 4a shows the lithiation/delithiation behavior of the C/Se composite in a Li–C/Se cell. In the first cycle, two lithiation plateaus centered at 1.6 V and 0.9 V, and a long slopping delithiation plateau centered at 1.8 V are observed. The lithiation plateau at 1.6 V and delithiation plateau at 1.8 V represent the redox reaction between Se and Li-ions, while the plateau at 0.9 V corresponds to the formation of a solid electrolyte interphase (SEI) layer and the lithiation of Se that is bonded with carbon. The low coulombic efficiency of the first cycle (65%) is due to the growth of SEI layer. In the second cycle, the coulombic efficiency increases to 94%, indicating a very small amount of newly formed SEI layer. In the second lithiation, the capacities of the plateaus at both 1.8 V and 0.9 V are reduced due to the dissolution of polyselenide caused by incompletely encapsulated Se. The physical encapsulation and chemical bonding of Se by carbon coating suppresses the volume expansion in the first few lithiation/delithiation cycles, which require an additional overpotential to overcome the stress/strain energy. After the activation process in few cycles, the deformation of the carbon matrix releases the stress/strain of the C/Se composite cathode, which shifts the lithiation/delithiation potential to a higher value. After 20 cycles, the lithiation plateau at 0.9 V becomes very short, while the lithiation plateau at 1.6 V shifts to 1.9 V with a higher capacity, demonstrating that most of the Se is activated. The delithiation plateau at 1.8 V also shifts to 1.95 V. The positive shift of both the lithiation and delithiation plateaus indicates the relief of the strain/stress in the composite upon cycling. The cyclic voltammogram (CV) scans in Fig. 4b confirm that there is only one pair of redox peaks during the lithiation/delithiation process. The cathodic peak is at 1.6 V in the first scan, and then it shifts to 1.7 V in the subsequent cycles, while the anodic peak is at 1.83 V with a little positive shift upon cycling. The sharp cathodic peak at 0.8 V represents the formation of a solid electrolyte interphase (SEI) layer and the cleavage of C–Se bond by electrochemical reaction between Se and Li-ion. The strong cathodic peak at 0.8 V is recovered in the second and third cycles, demonstrating that the contribution of the growth of the SEI layer is very small because the growth of the SEI layer mainly occurs in the first cycle. Fig. 3c and d show the cycle life and rate capability of the *in situ* formed C/Se composites. The composites deliver a charge capacity of 560 mA h g^{-1} at a current density of 100 mA g^{-1} in the first cycle, and retain the reversible capacity of 430 mA h g^{-1} after 250 cycles. In addition to a superior cycling stability, the composites also exhibit an excellent rate capacity. As shown in Fig. 3d, the reversible capacity of the composite is 600 mA h g^{-1} at a current density of 40 mA g^{-1}, while the reversible capacity remains at 280 mA h g^{-1} when the current density increases to 1.2 A g^{-1}, and the reversible capacity recovers to 600 mA h g^{-1} after the current density decreases back to 40 mA g^{-1}. Therefore, the exceptional electrochemical performance of the C/Se composite demonstrates that it is a promising cathode for rechargeable lithium batteries.

It was reported that Se cathodes have two potential plateaus at ~2.3 V and 3.75 V during delithiation.[23] The plateau at ~2.3 V corresponds to the conversion of Li_2Se to Se, whereas the plateau at 3.75 V is attributed to the redox shuttle reaction, triggered by the dissolution of polyselenide species in the electrolyte upon cycling. If the dissolution of polyselenide species can be avoided, the plateau at 3.75 V will disappear. Only one plateau at ~2.0 V was reported for the carbon encapsulated Se cathode[26] because the small pores of mesoporous carbon confine the polyselenide species and avoid the dissolution. In our work, Se is bonded and encapsulated by carbon such that the polyselenide species are restrained by the carbon matrix, thus the plateau at 3.75 V which is associated with the shuttle effect is not observed.

The phase structure of the C/Se electrodes before cycling and after fully lithiation/delithiation was characterized using XRD and Raman measurements, as shown in Fig. S2.† The fully

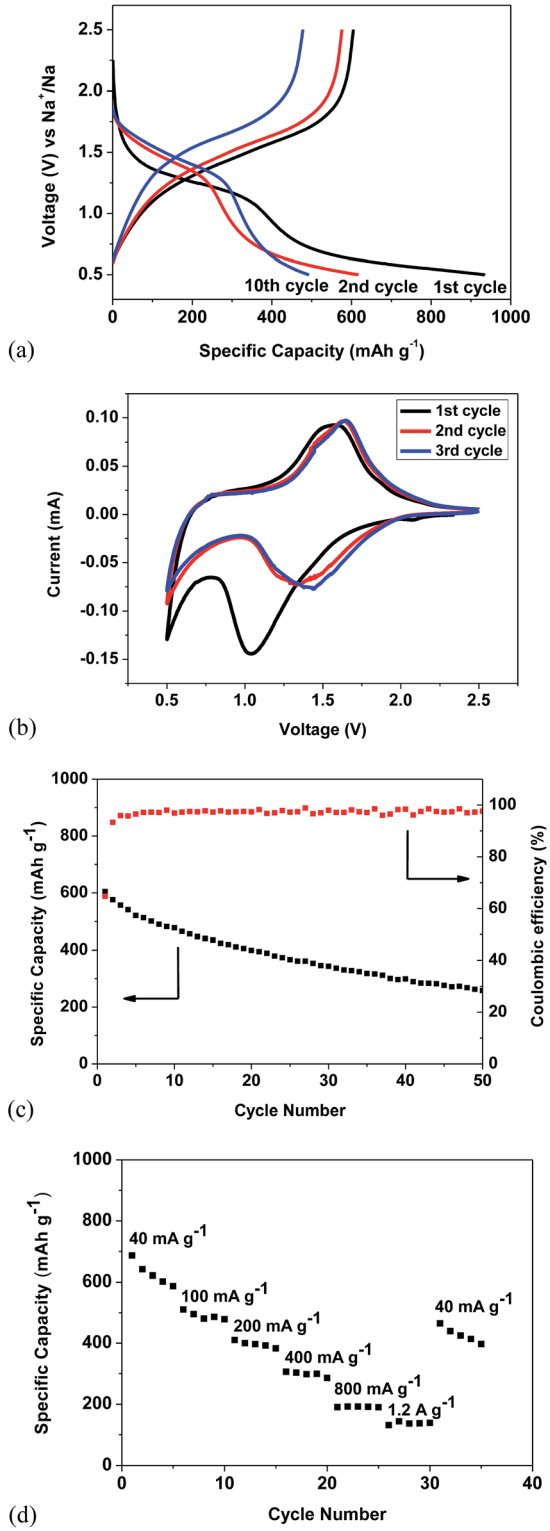

Fig. 5 Electrochemical performance of the *in situ* formed C/Se composite. (a) The galvanostatic charge–discharge curves between 0.5 V and 2.5 V *versus* Na/Na^+; (b) cyclic voltammograms at 0.1 mV s^{-1} in the potential window from 0.5 V to 2.5 V *versus* Na/Na^+; (c) desodiation capacity and coulombic efficiency *versus* cycle number at the current density of 100 mA g^{-1}; and (d) rate performance at various C-rates.

discharged C/Se electrode was prepared by disassembling the Li–C/Se cell in an Ar filled glovebox after discharging the cell to 0.8 V and maintaining it at 0.8 V for 24 h. The fully charged C/Se electrode was prepared after charging the electrode to 3.0 V and maintaining it at 3.0 V for 24 hours. Both electrodes were immersed in dimethyl carbonate for 24 h to remove $LiPF_6$ salt before the XRD and Raman measurements. The fresh C/Se electrode shows typical characteristic XRD peaks. All the characteristic XRD peaks of Se disappear in the fully discharged C/Se electrode, demonstrating that the lithiated Se becomes amorphous Li_2Se after complete lithiation. However, the characteristic XRD peaks of Se recover after complete delithiation, demonstrating that the crystalline structure of Se recovers upon cycling. The formation of Li_2Se after the full lithiation of the C/Se cathodes was also reported in the previous studies.[23,26] The Raman spectra of the fresh and cycled C/Se electrodes are shown in Fig. S2b.† In the fresh electrode, two broad carbon peaks at 1345 cm^{-1} and 1595 cm^{-1} can be observed, and the characteristic peak for cyclic Se_8 disappears due to the encapsulation and bonding of Se by the carbon matrix. After one change/discharge cycle, a small peak at 256 cm^{-1}, representing the chain-structured Se_n appears. The formation of the chain-structured Se_n after the first cycle enhances the electrochemical stability of the C/Se composite.

The unique C/Se composite can also be used as a cathode for sodium ion batteries. Fig. 5 shows the charge/discharge profiles of the C/Se composite in $NaClO_4$ EC/DMC electrolyte. The different behaviors of the C/Se composite for lithiation/delithiation and sodiation/desodiation are due to the different ion sizes and different potentials between Li metal and Na metal.[38] Firstly, the volume change induced by sodium ion insertion/extraction is considerably larger than lithium ion due to the larger size of sodium ion than that of the lithium ion. The larger volume change results in severe particle pulverization, which is a main reason for the capacity fading. Secondly, the potential of sodium metal (referring to a standard hydrogen electrode) is 0.3 V lower than that of lithium metal, thus the sodiation/desodiation plateau of the C/Se composite is 0.3 V lower than the lithiation/delithiation plateau. In Fig. 5a, two plateaus centered at 1.3 V and 0.6 V are observed during the first sodiation, while one slopping plateau centered at 1.5 V is observed during the first desodiation, which are 0.3 V lower than the lithiation/delithiation plateaus in lithium ion batteries due to the lower potential of sodium metal than lithium metal. The plateau centered at 0.6 V becomes very short from 2nd cycle to 10th cycle, while the plateau centered at 1.5 V becomes longer from 2nd cycle to 10th cycle, demonstrating that most of the Se in C–Se composite is activated after 10 cycles. The positive shift of both the sodiation and desodiation plateaus indicates the relaxation of the strain/stress in the composite upon cycling. The CV scans in Fig. 5b show that there is only one pair of redox peaks during the sodiation/desodiation process. In the first scan, there is a broad cathodic peak at 1.05 V and a conspicuous cathodic peak at 0.5 V, corresponding to the two plateaus at 1.3 V and 0.6 V in the first sodiation curve, and an anodic peak at 1.55 V, corresponding to the plateau at 1.5 V in the first desodiation curve. In the following scans, both the cathodic peak at 1.05 V and anodic

peak at 1.55 V shift to positive values, and the intensity of the sharp cathodic peak at 0.5 V becomes weaker upon cycling, which is coincident with the changes in the charge/discharge profiles. The long term cycling performance and rate capability are shown in Fig. 5c and 5d. The *in situ* formed C/Se composites deliver a charge capacity of 605 mA h g^{-1} in the first cycle at a current density of 100 mA g^{-1}, while it decreases to 258 mA h g^{-1} after 50 cycles. The cycle life in sodium cell is poorer than that in lithium ion cell due to the more severe volume change induced by the larger size of sodium ion. When the current density increases from 40 mA g^{-1} to 1.2 A g^{-1}, the desodiation capacity remains at 138 mA h g^{-1}. Therefore, the good electrochemical performance of the *in situ* formed C/Se composite paves the way for the feasibility of high-performance Na-ion batteries.

Conclusions

In conclusion, carbon bonded and encapsulated C/Se composites with 54% of Se were synthesized by the *in situ* carbonization of a mixture of PTCDA and Se in a sealed vacuum glass tube. The unique synthesizing technique enables the physical encapsulation and chemical bonding of Se by carbon, which greatly enhances the charge/discharge cycling stability in both lithium and sodium batteries. The exceptional electrochemical performance of the *in situ* formed C/Se composite demonstrates that it is a promising cathode material for rechargeable lithium and sodium batteries.

Acknowledgements

This work was supported by the Army Research Office under contract No. W911NF1110231. We acknowledge the support of the Maryland NanoCenter and its NispLab. The NispLab is supported in part by the NSF as a MRSEC Shared Experimental Facility. We acknowledge Kaitlyn Crawford, Prof. Lawrence R. Sita and Dr. Karen Gaskell for their technical support.

Notes and references

1 J. B. Goodenough and Y. Kim, *Chem. Mater.*, 2010, **22**, 587–603.
2 B. L. Ellis, K. T. Lee and L. F. Nazar, *Chem. Mater.*, 2010, **22**, 691–714.
3 B. Kang and G. Ceder, *Nature*, 2009, **458**, 190–193.
4 Y. Zhu, Y. Xu, Y. Liu, C. Luo and C. Wang, *Nanoscale*, 2013, **5**, 780–787.
5 F. Wu, N. Li, Y. Su, L. Zhang, L. Bao, J. Wang, L. Chen, Y. Zheng, L. Dai, J. Peng and S. Chen, *Nano Lett.*, 2014, **14**, 3550–3555.
6 S. J. Shi, Z. R. Lou, T. F. Xia, X. L. Wang, C. D. Gu and J. P. Tu, *J. Power Sources*, 2014, **257**, 198–204.
7 U. Kasavajjula, C. Wang and A. J. Appleby, *J. Power Sources*, 2007, **163**, 1003–1039.
8 X. Chen, J. Guo, K. Gerasopoulos, A. Langrock, A. Brown, R. Ghodssi, J. N. Culver and C. Wang, *J. Power Sources*, 2012, **211**, 129–132.
9 Y. Chen, X. Li, K. Park, J. Song, J. Hong, L. Zhou, Y. W. Mai, H. Huang and J. B. Goodenough, *J. Am. Chem. Soc.*, 2013, **135**, 16280–16283.
10 C. Wang, H. Wu, Z. Chen, M. T. McDowell, Y. Cui and Z. Bao, *Nat. Chem.*, 2013, **5**, 1042–1048.
11 S. Zheng, F. Yi, Z. Li, Y. Zhu, Y. Xu, C. Luo, J. Yang and C. Wang, *Adv. Funct. Mater.*, 2014, **24**, 4156–4163.
12 X. Ji, K. T. Lee and L. F. Nazar, *Nat. Mater.*, 2009, **8**, 500–506.
13 Y. Zhao, W. Wu, J. Li, Z. Xu and L. Guan, *Adv. Mater.*, 2014, **26**, 5113–5118.
14 A. Manthiram, Y. Fu and Y. Su, *Acc. Chem. Res.*, 2013, **46**, 1125–1134.
15 P. G. Bruce, S. A. Freunberger, L. J. Hardwick and J. M. Tarascon, *Nat. Mater.*, 2012, **11**, 19–29.
16 L. Suo, Y. S. Hu, H. Li, M. Armand and L. Chen, *Nat. Commun.*, 2013, **4**, 1481.
17 D. Wang, Q. Zeng, G. Zhou, L. Yin, F. Li, H. Cheng, I. R. Gentle and G. Q. Lu, *J. Mater. Chem. A*, 2013, **1**, 9382–9394.
18 J. Guo, Y. Xu and C. Wang, *Nano Lett.*, 2011, **11**, 4288–4294.
19 L. Ji, M. Rao, H. Zheng, L. Zhang, Y. Li, W. Duan, J. Guo, E. J. Cairns and Y. Zhang, *J. Am. Chem. Soc.*, 2011, **133**, 18522–18525.
20 H. Wang, Y. Yang, Y. Liang, J. T. Robinson, Y. Li, A. Jackson, Y. Cui and H. Dai, *Nano Lett.*, 2011, **11**, 2644–2647.
21 G. Zheng, Q. Zhang, J. J. Cha, Y. Yang, W. Li, Z. W. Seh and Y. Cui, *Nano Lett.*, 2013, **13**, 1265–1270.
22 H. Yao, G. Zheng, P. C. Hsu, D. Kong, J. J. Cha, W. Li, Z. W. Seh, M. T. McDowell, K. Yan, Z. Liang, V. K. Narasimhan and Y. Cui, *Nat. Commun.*, 2014, **5**, 3943.
23 A. Abouimrane, D. Dambournet, K. W. Chapman, P. J. Chupas, W. Weng and K. Amine, *J. Am. Chem. Soc.*, 2012, **134**, 4505–4508.
24 Y. Cui, A. Abouimrane, J. Lu, T. Bolin, Y. Ren, W. Weng, C. Sun, V. A. Maroni, S. M. Heald and K. Amine, *J. Am. Chem. Soc.*, 2013, **135**, 8047–8056.
25 Y. Cui, A. Abouimrane, C. J. Sun, Y. Ren and K. Amine, *Chem. Commun.*, 2014, **50**, 5576–5579.
26 C. Yang, S. Xin, Y. Yin, H. Ye, J. Zhang and Y. Guo, *Angew. Chem., Int. Ed.*, 2013, **52**, 8363–8367.
27 J. T. Lee, H. Kim, M. Oschatz, D. Lee, F. Wu, H. Lin, B. Zdyrko, W. Cho, S. Kaskel and G. Yushin, *Adv. Energy Mater.*, 2014, 4, DOI: 10.1002/aenm.201400981.
28 K. Han, Z. Liu, H. Ye and F. Dai, *J. Power Sources*, 2014, **263**, 85–89.
29 D. Kundu, F. Krumeich and R. Nesper, *J. Power Sources*, 2013, **236**, 112–117.
30 L. Liu, Y. Hou, X. Wu, S. Xiao, Z. Chang, Y. Yang and Y. Wu, *Chem. Commun.*, 2013, **49**, 11515–11517.
31 Z. Zhang, X. Yang, X. Wang, Q. Li and Z. Zhang, *Solid State Ionics*, 2014, **260**, 101–106.
32 Z. Zhang, Z. Zhang, K. Zhang, X. Yang and Q. Li, *RSC Adv.*, 2014, **4**, 15489–15492.
33 C. Luo, Y. Zhu, Y. Wen, J. Wang and C. Wang, *Adv. Funct. Mater.*, 2014, **24**, 4082–4089.
34 L. Liu, Y. Hou, Y. Yang, M. Li, X. Wang and Y. Wu, *RSC Adv.*, 2014, **4**, 9086–9091.

35 Z. Li, L. Yuan, Z. Yi, Y. Liu and Y. Huang, *Nano Energy*, 2014, **9**, 229–236.
36 C. Luo, Y. Xu, Y. Zhu, Y. Liu, S. Zheng, Y. Liu, A. Langrock and C. Wang, *ACS Nano*, 2013, **7**, 8003–8010.
37 J. F. Moulder, W. F. Stickle, P. E. Sobol and K. D. Bomben, *Handbook of X-ray Photoelectron Spectroscopy*, 1993.
38 H. Pan, Y. Hu and L. Chen, *Energy Environ. Sci.*, 2013, **6**, 2338–2360.